LETTERS
PUBLISHED ONLINE: 20 FEBRUARY 2017 | DOI: 10.1038/NMAT4856
nature materials

A non-volatile organic electrochemical device as a low-voltage artificial synapse for neuromorphic computing

Yoeri van de Burgt[1†‡], Ewout Lubberman[1,2‡], Elliot J. Fuller[3], Scott T. Keene[1], Grégorio C. Faria[1,4], Sapan Agarwal[3], Matthew J. Marinella[5], A. Alec Talin[3*] and Alberto Salleo[1*]

The brain is capable of massively parallel information processing while consuming only ∼1–100 fJ per synaptic event[1,2]. Inspired by the efficiency of the brain, CMOS-based neural architectures[3] and memristors[4,5] are being developed for pattern recognition and machine learning. However, the volatility, design complexity and high supply voltages for CMOS architectures, and the stochastic and energy-costly switching of memristors complicate the path to achieve the interconnectivity, information density, and energy efficiency of the brain using either approach. Here we describe an electrochemical neuromorphic organic device (ENODe) operating with a fundamentally different mechanism from existing memristors. ENODe switches at low voltage and energy (<10 pJ for 10^3 μm^2 devices), displays >500 distinct, non-volatile conductance states within a ∼1 V range, and achieves high classification accuracy when implemented in neural network simulations. Plastic ENODes are also fabricated on flexible substrates enabling the integration of neuromorphic functionality in stretchable electronic systems[6,7]. Mechanical flexibility makes ENODes compatible with three-dimensional architectures, opening a path towards extreme interconnectivity comparable to the human brain.

Two-terminal memristors based on filament-forming metal oxides (FFMOs) or phase change memory (PCM) materials have recently been demonstrated to function as non-volatile memory that can emulate neuronal and synaptic functions such as long-term potentiation (LTP), short-term potentiation (STP), and spike timing dependent plasticity (STDP)[4,5]. Crossbar architectures based on these devices have been projected to reduce energy costs for neural algorithms by six orders of magnitude, and recently performed image recognition and data classification when utilized as highly parallel neuromorphic processing units[8,9]. However, despite recent progress in the fabrication of device arrays, to date no architecture has been shown to operate with the projected energy efficiency while maintaining high accuracy. A major impediment still exists at the device level; specifically, a resistive memory device has not yet been demonstrated with adequate electrical characteristics to fully realize the efficiency and performance gains of a neural architecture. State-of-the-art memristors suffer from excessive write noise[10], write nonlinearities[8] and high write voltages and currents[11]. Reducing the noise and lowering the switching voltage significantly below 0.3 V (∼10 kT) in a two-terminal device without compromising long-term data retention has proven difficult[12]. These limitations reduce the accuracy and scalability of FFMO and PCM memristors and pose challenges for these devices to approach the energy efficiency of the brain[8].

Recognizing that different switching mechanisms may be beneficial, organic memristive devices have been recently proposed[13–15]. Besides low-cost manufacturing and flexibility inherent to soft materials, organic devices could also benefit from low-power consumption, added functionality, and biocompatibility. They could act as biometric sensors and direct interfaces with the brain[16,17], opening up the tantalizing opportunity to build advanced neural prostheses comprising integrated brain–machine interfaces that combine neural sensing with training[18]. However, the operation of these organic memristors relies either on the slow kinetics of ion diffusion through a polymer to retain their states or on charge storage in metal nanoparticles, which inherently limits performance and stability.

In contrast, the operation of ENODe is based on the non-volatile control of the conductivity of an organic mixed ionic/electronic conductor as depicted in Fig. 1. ENODe is essentially similar to a concentration battery. During the 'read' operation, the cell is disconnected and the electronic charge of the electrodes remains unaltered by virtue of an ion conducting/electron blocking electrolyte. The charge in the electrodes is manipulated during the 'write' operation. Hence, ENODe is a type of non-volatile redox cell (NVRC) in which the state of charge determines the electronic conductivity[19]. The main advantage of NVRCs is that the barrier for state retention is decoupled from the barrier for changing states, allowing for the extremely low switching voltages while maintaining non-volatility (Fig. 1c).

To demonstrate this concept, we use a poly(3,4-ethylenedioxythiophene):polystyrene sulfonate (PEDOT:PSS) film partially reduced with poly(ethylenimine) (PEI) (see Methods). The three-terminal device architecture comprises the postsynaptic electrode, a PEI/PEDOT:PSS film, interfaced with a PEDOT:PSS presynaptic electrode via an electrolyte (Fig. 1a). Upon applying a positive presynaptic potential V_{pre} to the PEDOT:PSS electrode, cations flow from the presynaptic electrode into the postsynaptic electrode through the electrolyte, resulting in protonation of the PEI, while electrons flow through the external circuit. This causes holes to be removed from the PEDOT backbone in the postsynaptic

[1]Department of Materials Science and Engineering, Stanford University, Stanford, California 94305, USA. [2]Zernike Institute for Advanced Materials, University of Groningen, 9747AG Gronigen, The Netherlands. [3]Sandia National Laboratories, Livermore, California 94551, USA. [4]Instituto de Física de São Carlos, Universidade de São Paulo, 13566-590 São Carlos, SP, Brasil. [5]Sandia National Laboratories, Albuquerque, New Mexico 87123, USA. [†]Present address: Microsystems and Institute for Complex Molecular Systems, Eindhoven University of Technology, 5612AJ Eindhoven, The Netherlands. [‡]These authors contributed equally to this work. *e-mail: aatalin@sandia.gov; asalleo@stanford.edu

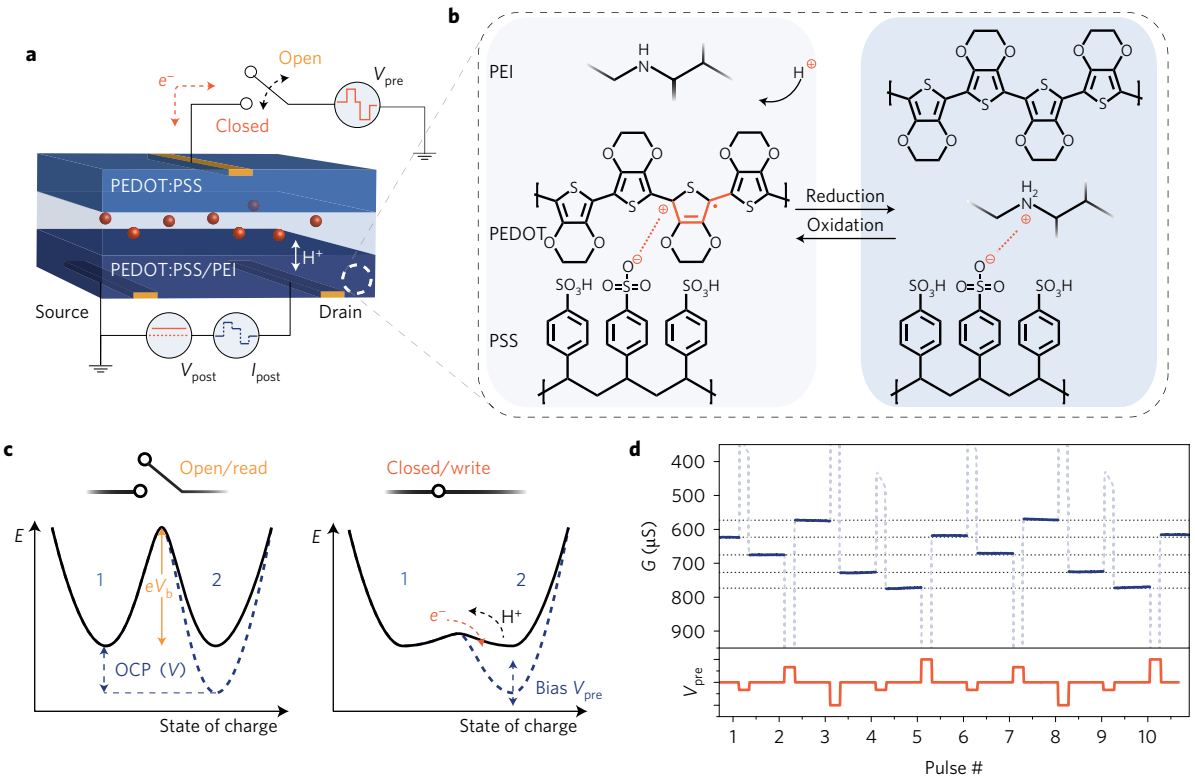

Figure 1 | Structure and electronic states of an organic neuromorphic device. a, Sketch of the device structure. Pre- and postsynaptic layers are separated by an electrolyte layer transporting ions/protons (red spheres). **b**, A positive V_{pre} drives protons into the postsynaptic electrode, which results in the compensation of some PSS^- by the protonated PEI. This reaction causes the reduction of PEDOT in the same electrode due to charge neutrality, which eliminates a polaron (in red) and decreases the polymer conductivity. The reaction is reversed upon applying a negative V_{pre}. **c**, Schematic explaining the decoupling of the read and write operations. NVRC ensures a very high eV_b barrier between the two oxidation states of PEDOT '1' and '2' (corresponding to two conductance states of the postsynaptic electrode) during an open read operation and a very low barrier during a closed write operation. The open circuit potential (OCP), depicted in dashed lines, is dependent on the oxidation state of PEDOT and can be overcome by the bias. **d**, Conductance G of the postsynaptic electrode, showing reproducible non-volatile switching between five discrete states.

electrode, thereby reducing its electronic conductivity while ensuring electroneutrality in the electrode (Fig. 1b). The reaction is reversed upon applying a negative V_{pre}. While enabling current continuity by ion transport, the electrolyte also acts as a barrier for electronic charge transport, maintaining the electrode conductance state after the presynaptic potential is applied. PEI stabilizes the neutral form of the PEDOT in the PEDOT:PSS/PEI electrode, ensuring that the oxidation state of the postsynaptic electrode is retained[20]. The conductance states are monitored using a postsynaptic potential V_{post}. As such, the conductance of the PEDOT:PSS/PEI channel represents the synaptic weight of the connection between two neurons[21], an essential property of an artificial synapse.

We show that ENODe exhibits some of the synaptic functions that are the building blocks of neuromorphic computing. To demonstrate the extremely high density of non-volatile states available for computation, a series of 500 pulses are applied (see Methods and Supplementary Information), resulting in 500 distinct conductance states (Fig. 2a). In addition to driving it with V_{pre}, ENODe can be operated by injecting a presynaptic current pulse (Fig. 2b) exhibiting a nearly perfect linear behaviour. We cycled ENODe between two distinct states over 300 times using 10 mV potentiation and depotentiation pulses, demonstrating extremely low noise (Supplementary Fig. 1) (<1%), which enables the definition of a large number of states in a small voltage range. The postsynaptic state is programmed by varying the amplitude or the duration of the presynaptic pulse. The conductance change, ΔG, is a linear function of presynaptic pulse amplitude and duration (Fig. 2d,e), down to approximately millisecond timescales (see inset).

Below 6 ms (>166 Hz) the potentiation is only short term (Supplementary Fig. 3). This timescale is consistent with a diffusion time constant, $\tau \sim L^2/D$ of ~10 ms, estimated using a previously measured charge carrier diffusivity in PEDOT:PSS of $\sim 10^{-8}$ cm^2 s^{-1} and an electrode thickness of ~100 nm (ref. 22). Reducing the channel thickness will reduce the diffusion distance and improve the time response. As sub-threshold potentiation in neurons is associated with STP and paired pulse facilitation (PPF), this functionality is also established in ENODe (Fig. 2c and Supplementary Fig. 2). Interestingly, the PPF demonstrated in Fig. 2c exhibits two characteristic timescales, $\tau_1 = 14$ ms and $\tau_2 = 240$ ms, approximately equal to those measured in biological synapses[23]. Additional bio-inspired functionality such as STDP can be achieved using overlapping pulse design (see Supplementary Information). Although STP is capacitive in nature, applying many short pulses results in LTP (Supplementary Fig. 3), a behaviour emulating short-term to long-term potentiation found in nature[24].

Size and geometry not only dictate operating speed, but also define switching energy. To highlight the path towards ultralow-energy switching of ENODe, power dissipation was measured in devices with areas spanning five orders of magnitude (see Fig. 2f). The power dissipated is determined by $P = I \times V$, and the energy is calculated by integration over the pulse width (Supplementary Fig. 4a). The switching energy of our smallest device was measured to be ~10 pJ, which is comparable to state-of-the-art PCMs that are over three orders of magnitude smaller, demonstrating the

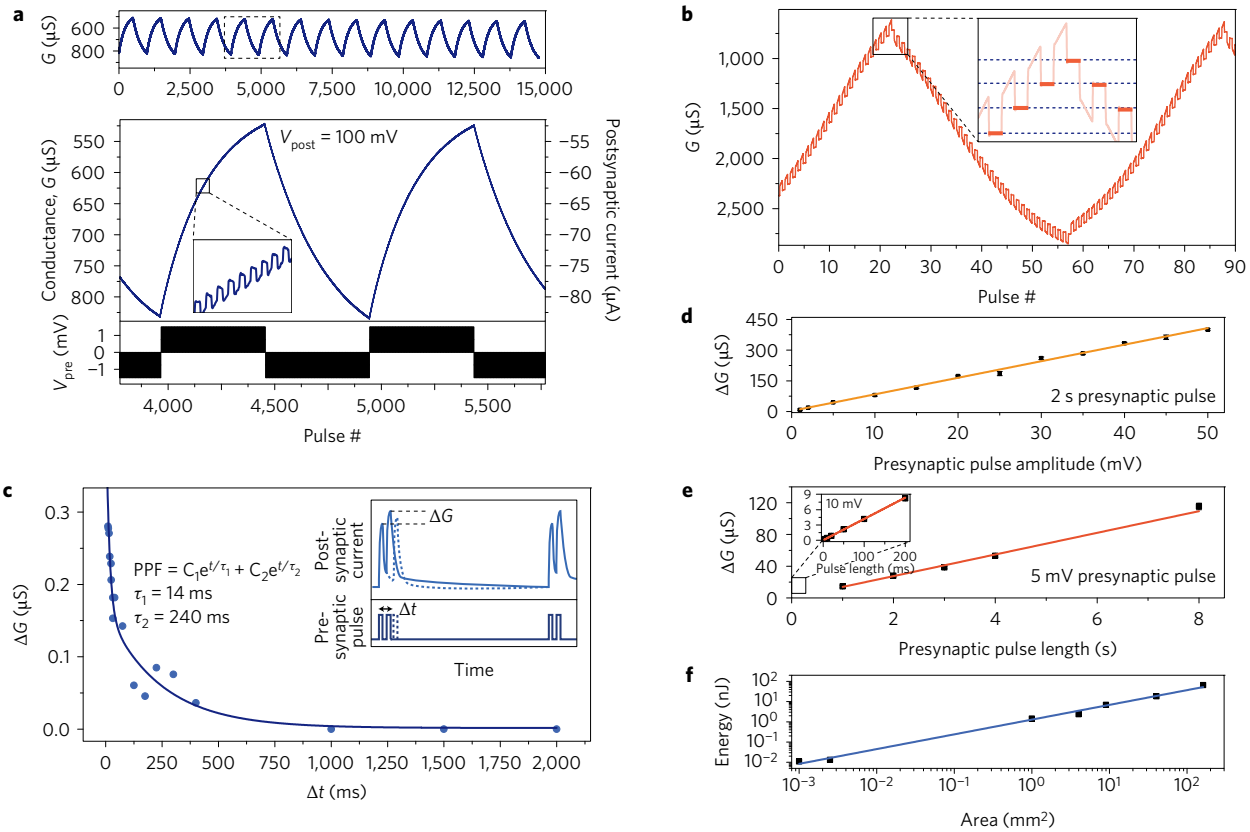

Figure 2 | Neuromorphic behaviour. a, Long-term potentiation and depression displaying 500 discrete states over the operating range when the device is controlled using voltage pulses. The inset is a zoom-in showing the individual states. **b**, Long-term potentiation and depression under current control. **c**, Short-term potentiation and paired pulse facilitation. The amount by which the synaptic weight is temporarily modified depends on the time interval between two short pulses. An exponential fit is applied to obtain two characteristic timescales. The inset is a schematic of how such biasing is typically realized. **d**,**e**, Change in postsynaptic conductance as a function of presynaptic pulse amplitude (**d**) and duration (**e**). The inset in **e** shows the relationship for shorter timescales and V_{pre} = 10 mV. **f**, Switching energy measured as a function of device area. Linear fits are applied in **d** to **f**.

particularly low switching energy density of ENODe[25]. Since current scales with area whereas the voltage, determined by the electrochemical overpotential at the polymer/electrolyte interface, remains approximately constant, the switching energy is proportional to the electrode area, with a slope of 390 ± 10 pJ mm^{-2} (Fig. 2f). Thus, we project an energy cost of 35 aJ for switching a 0.3 × 0.3 μm device, which can be fabricated by photolithography[26]. Downscaling of ENODe will also require that more resistive PEDOT:PSS formulations be used. We demonstrated using such formulations to fabricate devices with conductances ranging over three orders of magnitude (see Supplementary Information and Supplementary Figs 5,6). The energy advantage of ENODe is further enhanced by the low switching voltage (∼0.5 mV), which greatly reduces the interconnect capacitive loss in arrays and is ∼×10^3 lower than the 'write' voltage for a typical memristor.

Taking advantage of processing techniques developed for commodity polymers, we fabricated an all solid-state plastic device. Nafion was used as the electrolyte, laminated between two flexible PEDOT:PSS films coated on polyethylene terephthalate (PET) sheets and permeated with PEI (Fig. 3). This all-plastic device proves the potential for low-cost fabrication of flexible ENODe arrays, which would enable the integration of on-board neuromorphic computing and learning in implantable prosthetics, neural electrode arrays or any other flexible large-area electronic system[17]. Furthermore, bending and folding of arrays may enable three-dimensional densely connected neuromorphic devices.

As a first simple demonstration of functionality, we integrated ENODe in a circuit that emulates Pavlovian learning[27] (Fig. 4a and Supplementary Information). The output neuron N3 (salivation) is triggered by the input neuron N1 (sight of food, panel 1) but initially not by neuron N2 (bell ringing, panel 2). The synaptic weight of ENODe (S2) is modified during learning, thereby permanently associating N2 to N1 (panel 3). The learning process resulted in a response at N3 (salivation), to the input N2 (bell ringing), successfully demonstrating associative memory of our artificial synapse (panel 4).

Further, to fully illustrate the power of the low noise and linearly programmable conductance states of ENODe, we simulated a neural network based upon its experimentally measured properties (see Supplementary Information). We simulated a three-layer network for training with back-propagation of three data sets: an 8 × 8 pixel image version of handwritten digits[28]; MNIST, a 28 × 28 pixel version of handwritten digits[29]; and a Sandia file classification data set[30]. Back-propagation is a well-studied method that provides benchmarking with the data sets we used[8]. The numerical weights in the network layer were mapped directly onto the experimental device conductance states (Fig. 2a) that are extracted from ∼15,000 experimentally measured states. Training a neural network using ENODe gives an accuracy between 93% and 97%, and is always within 2% of the ideal floating-point-based neural network performance, which is the theoretical limit for this algorithm (Fig. 4d–f). Using a similar algorithm on PCM devices previously yielded far lower classification accuracies[8]. The key to this exceptional performance is the linearity and low noise of ENODe (Fig. 2d,e), allowing extremely efficient analog tuning[31]. In contrast, the physics of switching PCMs and FFMOs imposes

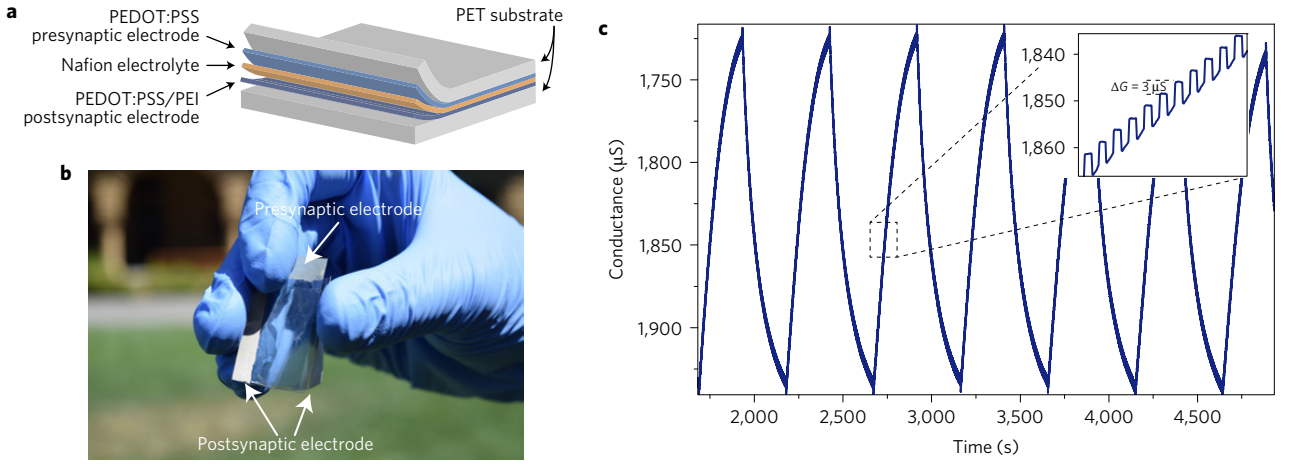

Figure 3 | Flexible all solid-state neuromorphic device. a, Schematic of the device. **b**, Photograph of the device while being flexed. **c**, 125 potentiation and depotentiation states obtained with 0.5 mV pulses. The inset shows the conductance difference between contiguous states.

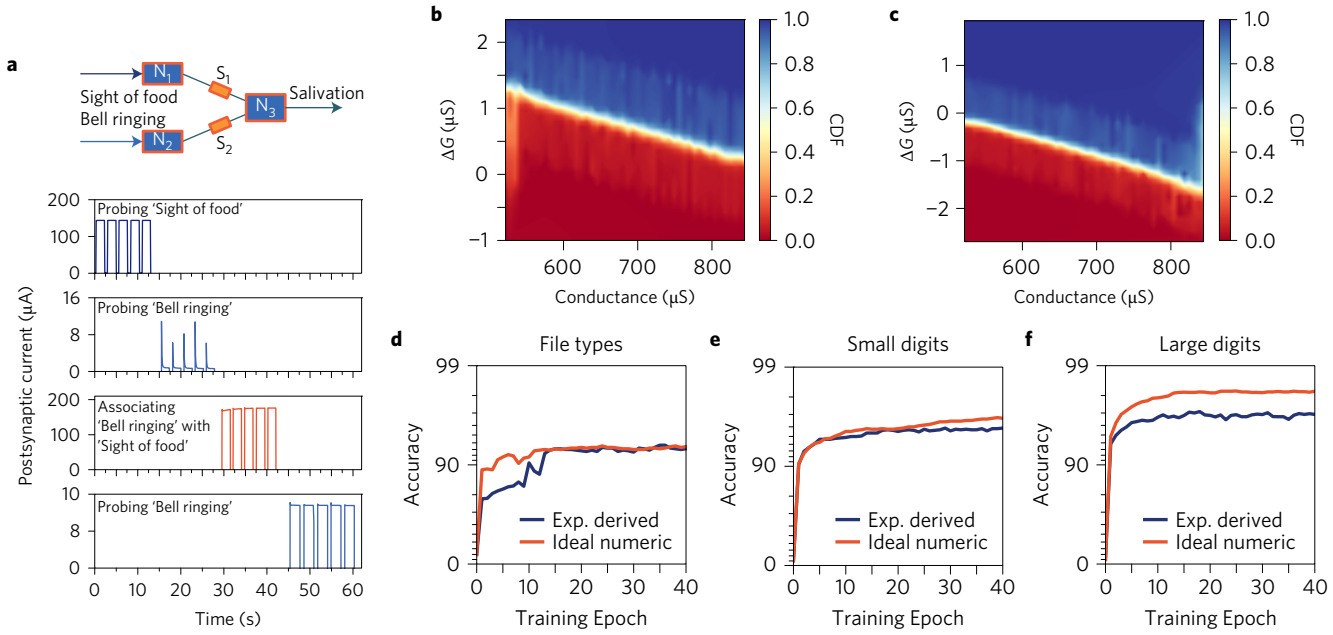

Figure 4 | Learning circuit and image recognition simulations. a, Schematic and results of the Pavlovian learning circuit. Conditioning and permanent association are shown in the third and fourth panel. **b**,**c**, Heat map representation of the ΔG versus G switching statistics of ENODe during potentiation (**b**) and depotentiation (**c**). The heat maps encompass data from 15,000 measurements and their colour represents the cumulative distribution function (CDF) at each conductance state. CDF is the probability that ΔG is less or equal to the ΔG plotted. **d**–**f**, Backpropagation training results using a Sandia file classification data set (**d**), an 8 × 8 pixel handwritten digit image (**e**) and a 28 × 28 pixel handwritten digit image (**f**).

inherently nonlinear device characteristics as it relies on random nucleation events (PCM) or on modulating a tunnel barrier over a narrow region (FFMO)[8,10].

Analog tuning and extremely low switching voltages are consistent with the inherently fast and low-energy process of ion transport into a swollen polymer, requiring only a small electrochemical overpotential[32]. We compared the composition of the pre- and postsynaptic electrodes before and after operation in liquid electrolyte (KCl) using X-ray photoelectron spectroscopy (XPS) and propose that cations from the supporting electrolyte (K^+) are mobile in the presynaptic electrode whereas protons (H^+) are the mobile species in the postsynaptic electrode (see Methods and Supplementary Information). Thus, upon applying a positive V_{pre}, K^+ cations are emitted from the presynaptic electrode into the electrolyte. As a consequence of this increase in positive charge concentration in the electrolyte, protons penetrate the PEDOT:PSS/PEI postsynaptic electrode and protonate amine groups in the PEI, which due to charge neutrality reduces the concentration of $PEDOT^+$, decreasing its conductivity. The opposite process occurs upon applying a negative V_{pre}.

The mechanism, which differs fundamentally from that of organic neuromorphic devices reported to date, explains the origin of the non-volatile nature of the conductance states of our device[13,14]. Electroneutrality in the device imposes that any charging caused by biasing the presynaptic electrode is balanced by an equal doping/dedoping in the postsynaptic electrode, resulting in a continuous analog tuning of the ENODe conductivity. Upon programming the device to a specific state, the presynaptic PEDOT:PSS electrode and the postsynaptic PEDOT:PSS/PEI film are at different potentials caused by the different $PEDOT^+$ concentration. Once programmed, the electrodes are disconnected from sources of charge and have no direct electrical connection to each other either since the electrolyte

is not an electrical conductor. Although random diffusion of a cation into the electrolyte could cause the erasing of a state, such a process would leave an uncompensated anion in the film. The stable, non-volatile states originate from the extremely large electrostatic barrier that the uncompensated anion would impose, typically observed in battery electrodes without connection to a load. State stability is indeed clearly established in retention measurements, showing a 0.04% standard deviation in conductance measured over 25 h (See Supplementary Information).

Interestingly, the working mechanism of ENODEs is reminiscent of that of natural synapses, where neurotransmitters diffuse through the cleft, inducing depolarization due to ion penetration in the postsynaptic neuron. In contrast, other memristive devices switch by melting materials at relatively high temperatures (PCMs) or by voltage-induced breakdown/filament formation and ion diffusion in dense oxide layers (FFMOs).

In conclusion, we demonstrate a new organic electronic device made with inexpensive and commercially available plastic materials that behaves as an artificial synapse. Our artificial synapse exhibits a large number of non-volatile and reproducible states (>500) and operates at very low voltages. We determined experimentally that our artificial synapse switches with low energy density and we project that just ~35 aJ is sufficient to switch a sub-micron device, a number smaller than that of biological synapses. Circuit simulations show that networks based on these synapses perform near the theoretical limit. The polymeric nature of the synapse opens up a range of novel applications where biological integration, flexibility and low cost provide unique opportunities for the adoption of these devices.

Methods

Methods, including statements of data availability and any associated accession codes and references, are available in the online version of this paper.

Received 21 September 2016; accepted 12 January 2017; published online 20 February 2017

References

1. Merkle, R. Energy limits to the computational power of the human brain. *Foresight Update 6* (Foresight Institute, 1989); https://www.foresight.org/Updates/Update06/Update06.1.html
2. Laughlin, S. B., de Ruyter van Steveninck, R. R. & Anderson, J. C. The metabolic cost of neural information. *Nat. Neurosci.* **1,** 36–41 (1998).
3. Merolla, P. A. *et al*. A million spiking-neuron integrated circuit with a scalable communication network and interface. *Science* **345,** 668–673 (2014).
4. Strukov, D. B., Snider, G. S., Stewart, D. R. & Williams, R. S. The missing memristor found. *Nature* **453,** 80–83 (2008).
5. Kim, S. *et al*. Experimental demonstration of a second-order memristor and its ability to biorealistically implement synaptic plasticity. *Nano Lett.* **15,** 2203–2211 (2015).
6. Chortos, A., Liu, J. & Bao, Z. Pursuing prosthetic electronic skin. *Nat. Mater.* **15,** 937–950 (2016).
7. Yokota, T. *et al*. Ultra-flexible organic photonic skin. *Sci. Adv.* **2,** e1501856 (2016).
8. Burr, G. W. *et al*. Experimental demonstration and tolerancing of a large-scale neural network (165,000 synapses) using phase-change memory as the synaptic weight element. *IEEE Trans. Electron Devices* **62,** 3498–3507 (2015).
9. Prezioso, M. *et al*. Training and operation of an integrated neuromorphic network based on metal-oxide memristors. *Nature* **521,** 61–64 (2015).
10. Yang, J. J., Strukov, D. B. & Stewart, D. R. Memristive devices for computing. *Nat. Nanotech.* **8,** 13–24 (2013).
11. Wong, H. S. P. *et al*. Phase change memory. *Proc. IEEE* **98,** 2201–2227 (2010).
12. Zhou, Y. & Ramanathan, S. Mott memory and neuromorphic devices. *Proc. IEEE* **103,** 1289–1310 (2015).
13. Gkoupidenis, P., Schaefer, N., Garlan, B. & Malliaras, G. G. Neuromorphic functions in PEDOT:PSS organic electrochemical transistors. *Adv. Mater.* **27,** 7176–7180 (2015).
14. Xu, W., Min, S.-Y., Hwang, H. & Lee, T.-W. Organic core-sheath nanowire artificial synapses with femtojoule energy consumption. *Sci. Adv.* **2,** e1501326 (2016).
15. Alibart, F. *et al*. A memristive nanoparticle/organic hybrid synapstor for neuroinspired computing. *Adv. Funct. Mater.* **22,** 609–616 (2012).
16. Jonsson, A. *et al*. Bioelectronic neural pixel: chemical stimulation and electrical sensing at the same site. *Proc. Natl Acad. Sci. USA* **113,** 9440–9445 (2016).
17. Larsson, K. C., Kjäll, P. & Richter-Dahlfors, A. Organic bioelectronics for electronic-to-chemical translation in modulation of neuronal signaling and machine-to-brain interfacing. *Biochim. Biophys. Acta* **1830,** 4334–4344 (2013).
18. Simon, D. T. *et al*. An organic electronic biomimetic neuron enables auto-regulated neuromodulation. *Biosens. Bioelectron.* **71,** 359–364 (2015).
19. Thakoor, S., Moopenn, A., Daud, T. & Thakoor, A. P. Solid-state thin-film memistor for electronic neural networks. *J. Appl. Phys.* **67,** 3132–3135 (1990).
20. Xuan, Y., Sandberg, M., Berggren, M. & Crispin, X. An all-polymer-air PEDOT battery. *Org. Electron. Phys. Mater. Appl.* **13,** 632–637 (2012).
21. Bi, G. Q. & Poo, M. M. Synaptic modifications in cultured hippocampal neurons: dependence on spike timing, synaptic strength, and postsynaptic cell type. *J. Neurosci.* **18,** 10464–10472 (1998).
22. Jain, V., Yochum, H. M., Montazami, R. & Heflin, J. R. Millisecond switching in solid state electrochromic polymer devices fabricated from ionic self-assembled multilayers. *Appl. Phys. Lett.* **92,** 33304 (2008).
23. Zucker, R. S. & Regehr, W. G. Short-term synaptic plasticity. *Annu. Rev. Physiol.* **64,** 355–405 (2002).
24. Ohno, T. *et al*. Short-term plasticity and long-term potentiation mimicked in single inorganic synapses. *Nat. Mater.* **10,** 591–595 (2011).
25. Kim, I. S. *et al*. High performance PRAM cell scalable to sub-20 nm technology with below 4F2 cell size, extendable to DRAM applications. *2010 Symposium on VLSI Technology* 203–204 (IEEE, 2010).
26. Zhang, Y. *et al*. 30 nm channel length pentacene transistors. *Adv. Mater.* **15,** 1632–1635 (2003).
27. Ziegler, M. *et al*. An electronic version of Pavlov's dog. *Adv. Funct. Mater.* **22,** 2744–2749 (2012).
28. Bache, K. & Lichman, M. *UCI Machine Learning Repository* (University of California, School of Information and Computer Science, 2016).
29. Lecun, Y., Cortes, C. & Burges, C. J. C. Gradient-based learning applied to document recognition. *Proc. IEEE* **86,** 2278–2324 (1998).
30. Cox, J. A., James, C. D. & Aimone, J. B. A signal processing approach for cyber data classification with deep neural networks. *Proc. Comput. Sci.* **61,** 349–354 (2015).
31. Bichler, O. *et al*. Visual pattern extraction using energy-efficient '2-PCM Synapse'; Neuromorphic Architecture. *IEEE Trans. Electron Devices* **59,** 2206–2214 (2012).
32. Stavrinidou, E. *et al*. Direct measurement of ion mobility in a conducting polymer. *Adv. Mater.* **25,** 4488–4493 (2013).

Acknowledgements

A.S. gratefully acknowledges financial support from the National Science Foundation (Award #DMR 1507826). Y.v.d.B. was supported by the Keck Faculty Scholar Funds and the Neurofab at Stanford. S.T.K. was supported by the Stanford Graduate Fellowship fund. Help from J. Rivnay in making small devices is gratefully acknowledged. This work was supported in part by Sandia's Laboratory-Directed Research and Development (LDRD) Program under the Hardware Acceleration of Adaptive Neural Algorithms (HAANA) Grand Challenge. E.J.F. and A.A.T. were also supported by Nanostructures for Electrical Energy Storage (NEES-II), an Energy Frontier Research Center funded by the US Department of Energy, Office of Science, Basic Energy Sciences under Award number DESC0001160. Sandia National Laboratories is a multi-mission laboratory managed and operated by Sandia Corporation, a wholly owned subsidiary of Lockheed Martin Corporation, for the US Department of Energy's National Nuclear Security Administration under contract DE-AC0494AL85000. E.L. also acknowledges the support of Holland Scholarship, University of Groningen Scholarship for Excellent Students, Hendrik Muller Vaderlandschfonds, Schimmel Schuurman van Outerenstichting, Fundatie Vrijvrouwe van Renswoude te Delft, Fundatie Vrijvrouwe van Renswoude te 's Gravenhage, Marco Polo fund. G.C.F. acknowledges INCT/INEO, the Fundação de Amparo à Pesquisa do Estado de São Paulo (FAPESP) and the Brazilian National Council (CNPq/Science without Borders Project) for financial support through project numbers 2013/21034-0 and 201753/2014-6.

Author contributions

Y.v.d.B., E.L., A.A.T. and A.S. designed the experiments. Y.v.d.B., E.L., E.J.F., S.T.K. and G.C.F. collected and analysed data. S.A. and M.J.M. designed the back-propagation simulations. All authors discussed the results and contributed to the manuscript preparation. Y.v.d.B., E.L., E.J.F., A.A.T. and A.S. wrote the manuscript.

Additional information

Supplementary information is available in the online version of the paper. Reprints and permissions information is available online at www.nature.com/reprints. Correspondence and requests for materials should be addressed to A.A.T. or A.S.

Competing financial interests

The authors declare no competing financial interests.

Methods

Fabrication methods. The larger devices were prepared by spin-coating a PEDOT:PSS solution (Heraeus, Clevios PH 1000) on two indium tin oxide (ITO) patterned glass substrates. This solution also contained 5 wt% ethylene glycol (EG) to increase the PEDOT:PSS conductivity, 0.1 wt% dodecyl benzene sulfonic acid (DBSA) as a surfactant and 1 wt% (3-glycidyloxypropyl)trimethoxysilane (GOPTS) as a crosslinking agent to improve film stability. EG, DBSA and GOPTS were all used as obtained from Sigma Aldrich. After spin-coating, the films where baked at 120 °C for 10 min. Next, one of the PEDOT:PSS films was subjected to 5 min of branched polyethylenimine (M_w = 800, Sigma Aldrich) vapour (250 °C) and baked for another 10 min at 120 °C. The liquid electrolyte (100 mM NaCl or KCl) was used in a well, patterned in a polydimethylsiloxane (PDMS) mask. Solid-state devices were made using Nafion-117, 0.18 mm thickness, 0.90 meq g^{-1} exchange capacity (VWR International LLC) sandwiched between two PET substrates, with added glycol and sorbitol as surfactants. Smaller devices were fabricated using a femtosecond laser (Spectra Physics Ti:Sapphire, 808 nm, 500 mW, 10 kHz) ablation process by which wells were precisely defined in crosslinked Parylene C coated glass. The PEDOT:PSS solution was subsequently spin-coated in these wells.

Electrical characterization. Electrical characterization was done using a Keithley 2610 dual-channel measurement set-up, supplemented by an Agilent 33500B waveform generator and an Agilent DSO1022A oscilloscope, and interpreted with customized LabView software. The presynaptic electrode is connected to the postsynaptic electrode by a Keithley 2610 in series with a 1 MΩ resistance to ensure no unintentional discharging of the device. By applying potential pulses with similar amplitudes, the effective voltage drop over the device changes as a result of the change in conductivity of the device and its value relative to the 1 MΩ in series.

Materials characterization. XPS measurements where done using a PHI VersaProbe system at the Stanford Nano Shared Facilities. Depth profiles were obtained after C_{60} sputtering using a 20 nA current. Ultraviolet–visible spectroscopy was performed with an Ocean Optics Spectrometer.

Data availability. The data that support the findings of this study are available within the article and its Supplementary Information or from the authors, see author contributions for specific data sets.